Journal of Power Sources 195 (2010) 1177–1181

Contents lists available at ScienceDirect

Journal of Power Sources

journal homepage: www.elsevier.com/locate/jpowsour

Short communication

Dominant frequency of pressure drop signal as a novel diagnostic tool for the water removal in proton exchange membrane fuel cell flow channel

Jixin Chen*,[1]

Mechanical and Aerospace Engineering, University of California, Irvine, Irvine, CA 92697-3975, USA

ARTICLE INFO

Article history:
Received 17 July 2009
Received in revised form 2 September 2009
Accepted 2 September 2009
Available online 11 September 2009

Keywords:
PEM fuel cell
Diagnostic tool
Pressure drop
Dominant frequency
FFT
Water removal

ABSTRACT

In this work, a transparent assembly was self-designed and manufactured to perform ex situ experimental study on the liquid water removal characteristics in PEM fuel cell parallel flow channels. It was found that the dominant frequency of the pressure drop across the flow channels may be utilized as an effective diagnostic tool for water removal. Peaks higher than 1 Hz in dominant frequency profile indicated water droplet removals at the outlet, whereas relatively lower peaks (between 0.3 and 0.8 Hz) corresponded to water stream removals. The pressure drop signal, although correlated with the water removal at the outlet, was readily influenced by the two phase flow transport in channel, particularly at high air flow rates. The real-time visualization images were presented to show a typical water droplet removal process. The findings suggest that dominant frequency of pressure drop signal may substitute pressure drop as a more effective and reliable diagnostic tool for water removal in PEM fuel cell flow channels.

1. Introduction

The proton exchange membrane (PEM) fuel cell has been regarded as an ideal power source for a variety of applications due to its significant advantages, *i.e.*, high efficiency, low emission, silence and simplicity [1]. The water management in PEM fuel cell is one of the crucial issues to be fully understood and optimized before further advances could be made. Sufficient amount of water is necessary for maintaining the membrane ion conductivity whereas excess water, or water flooding, may block the pores of electrodes and the flow channels, thereby reducing the reactant mass transfer to catalytic sites [2–5]. The capacity to perform effective water removal, therefore, becomes one of the most important specifications for PEM fuel cell flow channels [6]. Since it is highly desired to know the water behavior in both flow channels and porous electrodes, many modeling studies have been conducted [7–10]. Several advanced considerations including two phase flow in channels and electrodes, wettability of gas diffusion layer (GDL) and transient processes in fuel cell have been covered in these modeling studies. On the other hand, numerous experimental works concern about the diagnostic tools for the water behavior in PEM fuel cell. Research in such aspect may proceed as a more straightforward and effective way to deal with the water management, since the objective is to sense or predict the flooding/drying accurately before applying corresponding actions. Particularly, transparent fuel cell was designed for direct in situ visualization of water transport and distribution in flow channels [11–13]. Due to the limited view field and water visualization effect, however, transparent fuel cell normally can apply straight parallel channel design only. In addition, the water transport and distribution under the land cannot be revealed under transparent fuel cell configuration. Neutron imaging technique was also utilized to obtain the water distribution profiles in PEM fuel cell [14–16], with a limitation that the precise location of water is difficult to determine due to the overlapping of images. Moreover, magnetic resonance imaging (MRI) technique turned out to be also an effective tool to capture the water behavior both in membrane and flow field [17–19]. Its weakness is principally in the requirement that the materials have to be nonmagnetic, making the water in the catalyst layer and GDL, either nonwoven carbon paper or woven carbon cloth, hard to visualize. A thorough review of these techniques can be found in Ref. [20]. In addition to direct visualization, indirect diagnostic tool usually is to monitor some easy-to-measure engineering parameters. Pressure drop across the flow channel was proposed to be a diagnostic tool for PEM fuel cell flooding by Bosco and Fronk in General Motors [21]; similar findings concerning pressure drop as a diagnostic tool were reported by Barbir et al. [22], Ma et al. [23] and Ito et al. [24]. Although other parameters, such as cell resistance [22] and electrode diffusivity [25], were also used as diagnostic tool, pressure drop as the mainstream one shows significant advantages, namely, the immediate and real-time linkage between the air–water two phase flow behavior and the pressure drop. Normally, a pressure

* Tel.: +1 949 824 0701; fax: +1 949 824 8585.
E-mail address: jixinc@uci.edu.
[1] Present address: Mechanical Engineering, University of Michigan, Ann Arbor, MI 48109, USA.

0378-7753/$ – see front matter © 2009 Elsevier B.V. All rights reserved.
doi:10.1016/j.jpowsour.2009.09.003

drop increase is considered a sign of water accumulation or water film build-up in the channel; whereas a sudden decrease indicates a water removal at the outlet. However, pressure drop as a diagnostic tool for the water behavior, particularly water removal, does have shortcomings: first, high frequency oscillation in pressure drop is usually observed, which comes from the unstable two phase flow transport in channel; such oscillation does not indicate any water removal/build-up at the outlet but make a regular increase/decrease pattern in pressure drop profile fairly hard to distinguish; second, considering the relatively low pressure drop (usually <1000 Pa) across fuel cell channels, signal noises from disturbances and measurement errors may contribute considerably to the results, reducing the accuracy and even changing the pattern of the pressure drop profile. Consequently, real-time visualization results are usually used to assist the interpretation of the pressure drop profiles.

Under such circumstance, the author attempted to find a more reliable and effective diagnostic tool for water removal. In performing fast Fourier transform (FFT) upon certain amount of pressure drop data, one can obtain the frequency spectrum determined by the absolute magnitude and phase. The normalized dominant frequency is defined as the weighed average of the three components with largest power magnitudes. Compared with simply using the pressure drop as the diagnostic tool, its dominant frequency provides more accurate and robust insights about the water removal, although the new diagnostic tool essentially comes from applying some special mathematical treatment on the original pressure drop signal.

2. Experimental

2.1. Experimental setup

In this work, an assembly resembling the transparent PEM fuel cell [11] was self-designed and precisely manufactured using CNC machine. It consists of an end plate with two parallel microchannels built on, a transparent plastic plate for visualization and a window plate to apply even compression to the whole assembly. Porous media (carbon foam) was inserted into the channels to simulate the effect of GDL intrusion in flow channel [26]. Necessary O-rings were placed on site to avoid leakage. The width of the channel is 1.5 mm and the depth 1.2 mm; consistent with typical fuel cell designs. The effective length of the channel is 40 mm, with an entrance region to stabilize the air flow. Since the core frictional pressure drop in the developing (entrance) region of the channel is non-linear and unstable [27], the pressure drop measurement was only performed on the effective length (40 mm) of the channel. Pressure measurement ports were precisely drilled at two ends of the channels. The experimental setup is schematically shown in Fig. 1, with a photo of the transparent assembly attached. The differential pressure across the whole channel was measured by a Setra 230 series transducer; data from the transducers were real-time displayed and recorded using self-developed LabVIEW programs. A CCD camera was attached to the microscope to capture the real-time water removal video at the outlet. Both de-ionized water and compressed air were injected into the channels to simulate the two phase flow in fuel cell. Liquid water was injected into each channel separately using a syringe pump, so that the injection rate can be accurately controlled. The water injection rate was set to 0.01 ml min^{-1} corresponding to liquid superficial velocity (U_l) of 0.093 m s^{-1} in each channel, which was an analogy to the generation rate in real fuel cell operation under a normal current density of 0.6 A cm^{-2} and an effective MEA area of 4 cm^2. Meanwhile, air flow rates were varied from 0.01 to 0.8 l min^{-1} using a mass flow controller, corresponding to stoichiometry ratios up to 10 in fuel cell operation, and gas superficial velocities (U_g) from 0.09 to 3.7 m s^{-1} in each channel.

2.2. Mathematical treatment

In this section, the author would like to present the method to obtain the dominant frequency from the pressure drop signal. Signals are converted from time domain to frequency domain through the Fourier transform. It converts the signal information to the magnitude and phase component of each frequency. Customarily the Fourier transform is further processed to obtain the power spectrum, which is the magnitude of each frequency component squared. The spectrum can be then studied to obtain information about which frequencies are present in the input signal and/or which are significant component in terms of the magnitude of power.

FFT is an efficient algorithm to compute the discrete Fourier transform (DFT). Let $x_0, \ldots x_{N-1}$ be complex numbers, the DFT is defined by [28]:

$$X_k = \sum_{n=0}^{N-1} x_n e^{(-j2\pi/N)nk} \quad k = 0, \ldots, k-1$$

Obviously, this algorithm is complicated to work out as it involves many additions and multiplications of complex numbers. FFT is another method for calculating the DFT. While it produces the same result, it is incredibly more efficient, often reducing the

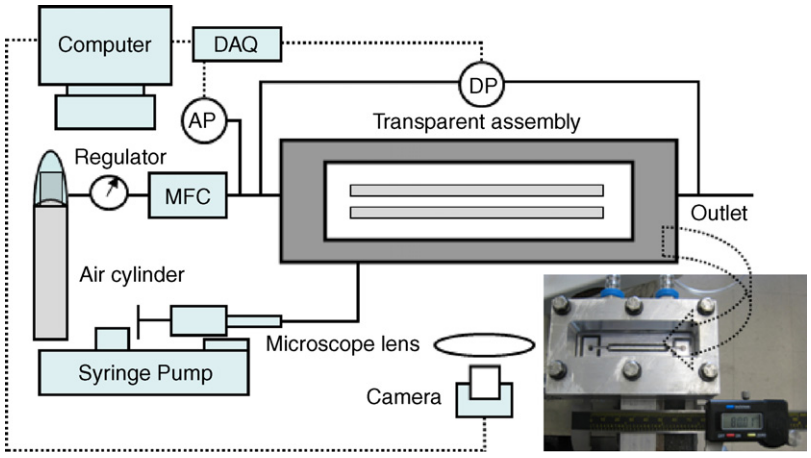

Fig. 1. Schematic of the experimental setup.

computation time by hundreds. The details of FFT algorithm are not presented here since it was performed simply by relevant MATLAB commands without knowing the internal workings. For the pressure drop signal in this work, it was sampled every 0.16 s and recorded in the data file. Therefore it can be considered a discrete data sequence and FFT can be performed, although the pressure drop itself was analog signal.

It is necessary to introduce two self-defined parameters. "Window" is the data to be processed together by FFT. The amount of such data is therefore termed "window size". One needs to determine how many data to be processed at one time (window size) so that the optimum power spectrum that facilitates analysis can be generated. Details for finding the appropriate window size are not presented here but can be found in Ref. [29]. Another parameter is defined to describe the major frequency component, which is of most significance in the pressure drop signal. The power spectrum obtained after performing FFT on the window will have numerous frequency components that show different power. The frequency with the maximum power obviously is the major component. However, considering only the frequency with the maximum power may be inappropriate, particularly when the second maximum power is very close to the maximum. Therefore, the normalized dominant frequency is defined as [29]:

$$\text{normalized dominant frequency} = f_1 \times \frac{P_1}{P_1+P_2+P_3} + f_2 \times \frac{P_2}{P_1+P_2+P_3} + f_3 \times \frac{P_3}{P_1+P_2+P_3}$$

where P_1 is the maximum power and f_1 the corresponding frequency, P_2, P_3 the second and third maximum power and f_2, f_3 the corresponding frequency, respectively. The normalized dominant frequency hence indicated the major frequency component of the pressure drop signal by taking into account the three frequencies with largest power magnitudes.

3. Results and discussion

3.1. Pressure drop profiles

In this section, the profiles of pressure drop across the channels are presented and analyzed. Fig. 2 shows the real-time profiles when the water was injected at 0.1 ml min^{-1}. Overall, higher air supply rate resulted in higher pressure drop. Apparent pressure drop oscillations were observed for air flow rate of 0.0566 l min^{-1}

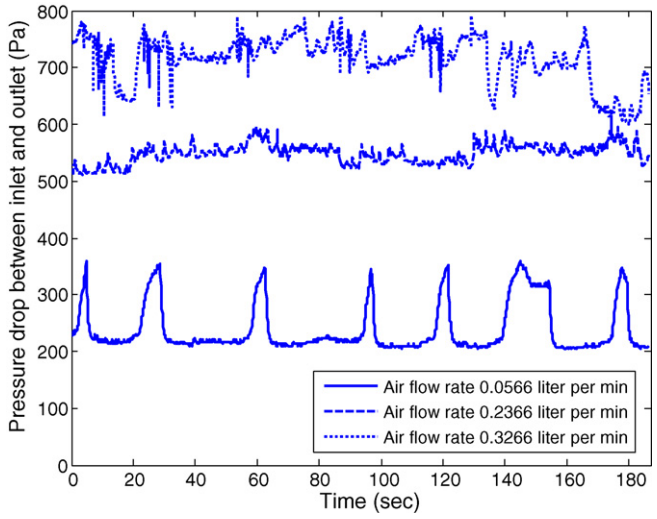

Fig. 2. Pressure drop profiles at water injection rate of 0.01 ml min^{-1} and different air flow rates.

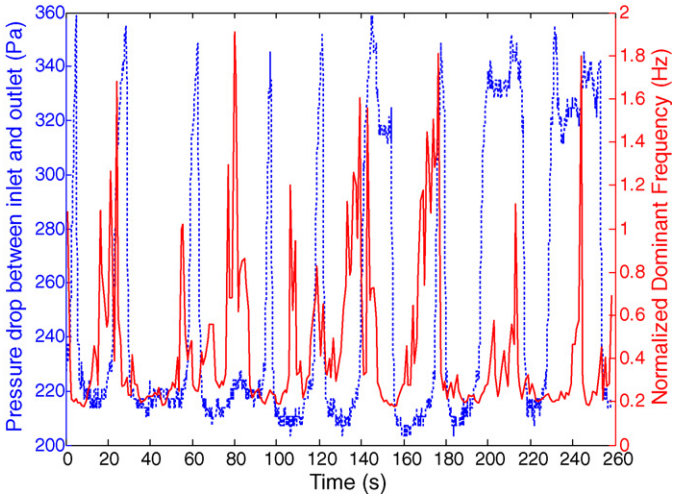

Fig. 3. Co-plot of dominant frequency and pressure drop against time at water injection rate of 0.01 ml min^{-1} and air supply rate of 0.0566 l min^{-1}.

(the solid line). Every peak in the oscillation indicated one removal of water droplet at the outlet, whereas the flat bottom of the oscillation corresponded to the injected water transport in the channel. As the water arrived at the outlet, it was not expelled out immediately by the air flow; instead, it was accumulating to form a droplet with a diameter of ~1.5 mm, the droplet was not expelled out until sufficient high pressure was gradually built up. The pressure drop sharply fell down as soon as the droplet was removed at the outlet. It should be noted that although the syringe pump ran continuously after the system started, the actual water injection via a 0.7 mm inner diameter hose was intermittent, *i.e.*, the water would not enter the channel until sufficient pressure build-up so that the injection style was droplet by droplet. The duration between two peaks in pressure drop profile equaled the sum of the waiting time between two droplet injections and the time for water to transport through the whole channel. However, as the air supply rate was increased (the dashed and dotted lines), the pressure drop profiles became much more coarse and irregular, making it extremely hard to obtain the water removal information solely from the pressure drop profile. At increased air flow rates, water could be readily removed whenever it reached the outlet; the pressure build-up/release cycle for water removal was no longer necessary. As a result, the water was expelled out in the form of stream, film or tiny droplet (stream being the majority), instead of large droplet (~1.5 mm diameter) as before. On the other hand, the unstable pressure drop signal highly correlated with the two phase flow transport in the channels. High rate air flow was strongly disturbed by the water presenting in channel, which explained the occurrence of many high frequency and irregular pressure drop oscillations. For these reasons, it may be impossible to read the water removal from the pressure drop oscillation as before. Pressure drop as the diagnostic tool thus saw some limitation at increased air flow rates. Visualization images were very necessary at such moment to assist the diagnosis.

3.2. Real-time dominant frequency plots

The normalized dominant frequency and the original pressure drop were co-plotted against time in Fig. 3 when the water injection rate was 0.01 ml min^{-1} and air supply rate 0.0566 l min^{-1}. To obtain the frequency profile, at any given time except the first second, the window was applied on certain amount (window size, in this case 36) of data right before the datum at that moment. Therefore, the

advance of frequency change to diagnose the water behavior could be guaranteed. Note that at the very beginning (the first second) of data recording, the window was applied on the data right after since no historical data available yet.

The water removal pattern in this case may be named "intermittent droplets mode". As clearly illustrated in Fig. 3, every time before the water removal, the dominant frequency experienced a peak together with the pressure drop. Also, the real-time visualization indicated that the magnitude of the peak in frequency correlated with the size of the water droplet that was removed at the outlet. For example, the ~1.8 Hz peak at about 80 s corresponded to the removal of a ~1.5 mm diameter droplet; whereas lower peak at about 25 s to smaller water droplet with diameter of ~1.0 mm. It is worthy to note the last two peaks in dominant frequency locating within the peaks of pressure drop, which are much wider than previous ones. The visualization indicated that during the wider peak in pressure drop, the water was accumulating and then forming droplet but differently, it was not expelled out as the droplet was formed; the droplet grew larger and eventually broken down into a series of small droplets (diameter ~0.3 mm), which then flowed out very quickly. The unique peak in dominant frequency during such process perfectly indicated the one removal of a series of small droplets and predicted the moment of removal (right after each peak). However, judging from the pressure drop profile, one may get confused at the wider peaks and incorrectly speculate that the water was removing during the whole peak.

A typical water removal process is presented in Fig. 4. The still images can only show part of the whole process with the critical scenes. Specific time for taking each scene is indicated so that a direct comparison can be made with profiles in Fig. 3. From Fig. 4(a) to (c), the pressure was gradually built up with water accumulation and droplet growth, during which the pressure drop profile experienced apparent uptrend. The edge of the formed droplet could be clearly seen in these figures. In Fig. 4(a), the water from the channels accumulated at the outlet; then a droplet was formed and began to vibrate (the unstable edges could be clearly seen in (b) and (c)). In Fig. 4(d) and (e), the water was promptly flowing out in droplet, corresponding to the abrupt pressure drop decrease around 180 s in Fig. 3.

Fig. 5 shows the dominant frequency and pressure drop co-plot when the air supply rate was increased to 0.2366 l min^{-1}. In this case, the water removal at the outlet was not so regular like previous case; the droplet formation and growing process were not frequently observed. Instead, the water was flowing out in stream for most of time, corresponding to many relatively lower dominant frequency peaks (0.4–0.6 Hz) in Fig. 5. The dominant frequency peak higher than 1.2 Hz indicated there was still one water removal in droplet (~1.0 mm diameter) at around 120 s, consistent with the visualization result. The increased air supply rate obviously made the water removal more chaos, as the increased air flow could readily provide the pressure needed to push out the water at the outlet. Consequently, instead of the intermittent mode in previous case, the water removal could be considered almost continuous, not completely because there were still low frequency regimes (<0.3 Hz) in Fig. 5. Examining the pressure drop profile, one cannot obtain the water removal information, since the pressure drop was influenced by the water transport in channel also; particularly at increased air flow rate, the instability effects were amplified. Fig. 6 presents the visualization image for water transport in channel at air supply rate of 0.2366 l min^{-1}, which may help the understanding of the unstable pressure drop. It can be seen that water transport occurred both in forming a film at the channel sides and in passing through the pores of porous media (a representative region shown in the ellipse). Such water transport in channel, no matter in either way, would disturb the air flow and considerably contribute to the instability of pressure drop profile. Therefore, although one could find many "peaks" in the pressure drop profile in Fig. 5, most of them were not from the water removal at the outlet but the unstable two phase flow, particularly the water transport in the channel. However for the frequency profile, the lower peaks (0.4–0.6 Hz) in dominant frequency indicated water removal at the outlet in form of stream and higher peak (>1.2 Hz) in form of droplet. The dominant frequency profile clearly shows advantages over pressure drop profile in diagnosis of water removal at the outlet.

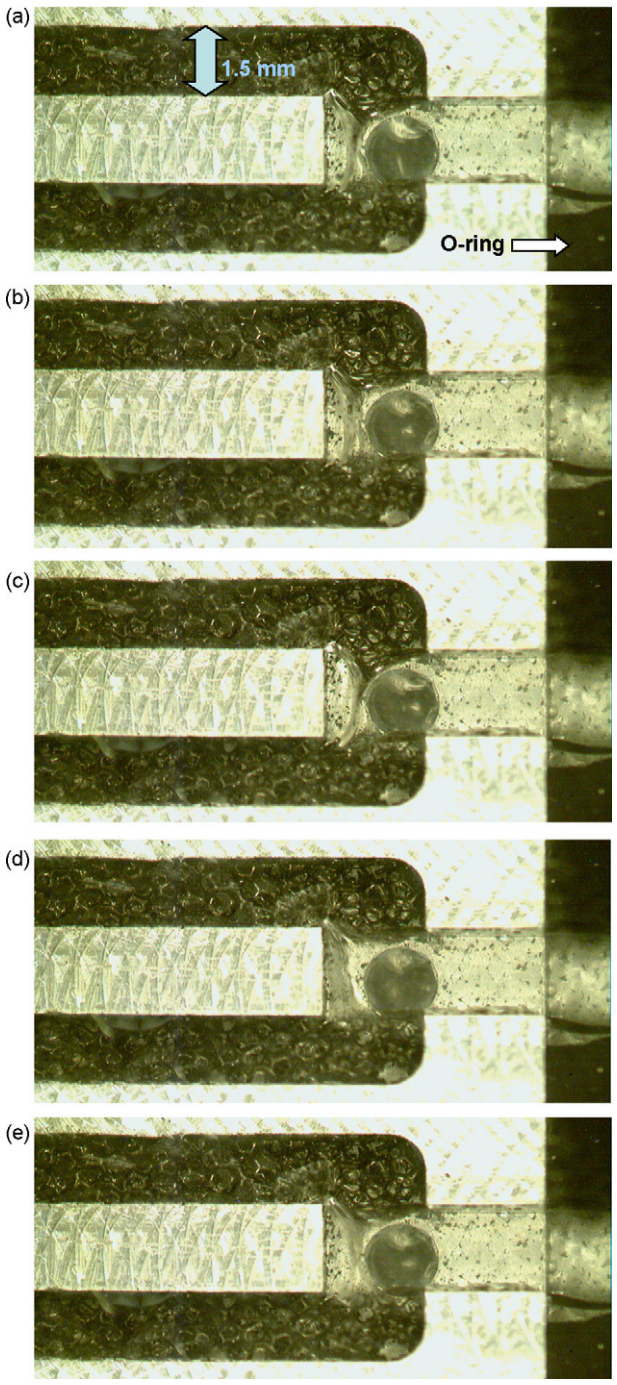

Fig. 4. Visualization images of a typical water removal process occurred at water injection rate of 0.01 ml min^{-1} and air supply rate of 0.0566 l min^{-1}: (a) water accumulation at t = 173.2 s; (b) droplet formation at t = 175.3 s; (c) pressure further build-up and droplet being pushed at t = 176.8 s; (d) the beginning of droplet removal at t = 178.3 s; (e) water removal and pressure release at t = 179.5 s.

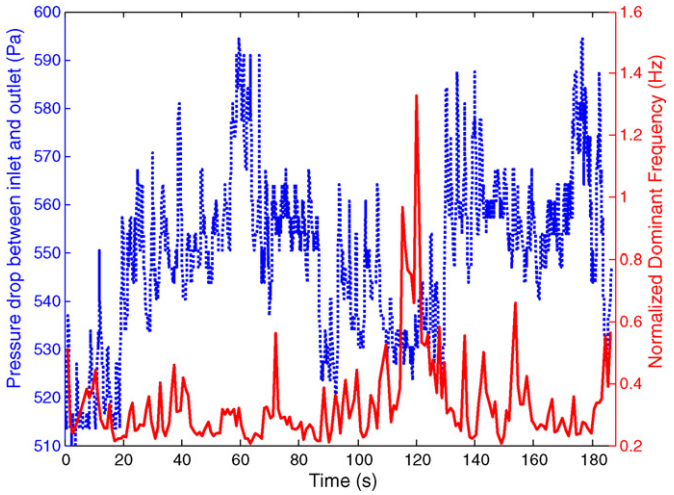

Fig. 5. Co-plot of dominant frequency and pressure drop against time at water injection rate of 0.01 ml min^{-1} and air supply rate of 0.2366 l min^{-1}.

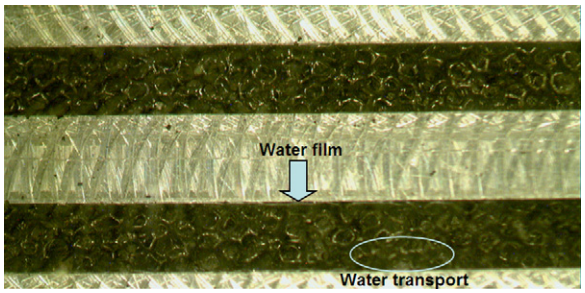

Fig. 6. Visualization image of the water transport in channel at water injection rate of 0.01 ml min^{-1} and air supply rate of 0.2366 l min^{-1}.

Fig. 7 shows the co-plot obtained at further increased air supply rate 0.3266 l min^{-1}. The pressure drop profile contains more intense oscillations as the water transport in channel became more unstable. However, applying the above criteria on the dominant frequency profile, one can still find that the water droplet removals took place at approximately 15, 45, 55, 85 and 185 s, and several water stream removals at other moments. Again, the dominant frequency as a diagnostic tool shows better reliability and resistance to noise than pressure drop, particularly at increased air flow rates.

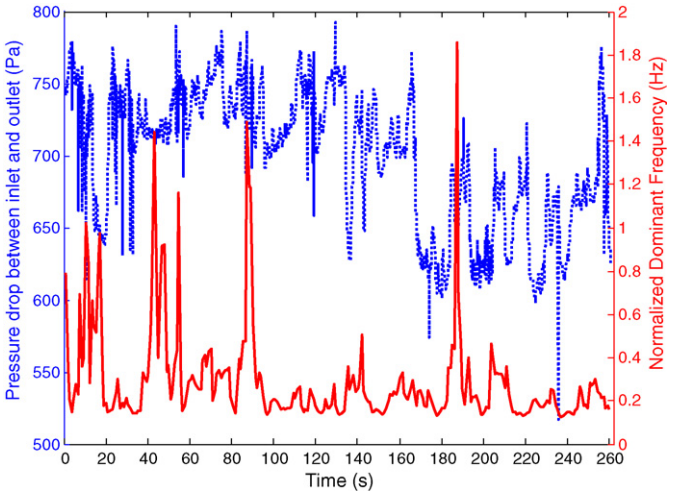

Fig. 7. Co-plot of dominant frequency and pressure drop against time at water injection rate of 0.01 ml min^{-1} and air supply rate of 0.3266 l min^{-1}.

4. Conclusions

In this study, the relations between the water removal in the PEM fuel cell parallel channels and the dominant frequency of pressure drop signal were experimentally investigated using a self-designed and manufactured transparent assembly. It was found that dominant frequency showed better performance in water removal diagnosis compared with pressure drop, which presently is the principal diagnostic tool for the water behavior. The real-time visualization results indicated that peaks higher than 1 Hz in dominant frequency corresponded to the water droplet removals (after its formation and growth) and peaks between 0.3 and 0.8 Hz corresponded to the water stream removals. Additionally, higher magnitude in dominant frequency peak corresponded to water droplet with larger size. The pressure drop across the channels may not diagnose the water removal accurately because it was readily influenced by the two phase flow transport in channel, although also correlated with the water removal at the outlet. Particularly at high air low rates, dominant frequency showed much better reliability and higher accuracy than pressure drop for water removal diagnosis. It may be preferred to use dominant frequency as an effective diagnostic tool for water removal in PEM fuel cells. Future work will mainly concern the establishment of a mathematical model correlating the dominant frequency and water removal characteristics such as droplet diameter and cycle duration.

Acknowledgments

Supports from Professor Yun Wang at Mechanical and Aerospace Engineering, UC Irvine are gratefully acknowledged.

References

[1] J. Larminie, A. Dicks, Fuel Cell System Explained, John Wiley & Sons, 2003, pp. 22–29.
[2] Z.H. Wang, C.-Y. Wang, K.S. Chen, J. Power Sources 94 (2001) 40–50.
[3] U. Pasaogullari, C.-Y. Wang, J. Electrochem. Soc. 151 (2004) A399–A406.
[4] X. Yu, B. Zhou, A. Sobiesiak, J. Power Sources 147 (2005) 184–195.
[5] F.Y. Zhang, X.G. Yang, C.-Y. Wang, J. Electrochem. Soc. 153 (2006) A225–A232.
[6] X. Li, I. Sabir, Int. J. Hydrogen Energy 30 (2005) 359–371.
[7] H. Meng, C.-Y. Wang, J. Electrochem. Soc. 152 (2005) A1733–A1741.
[8] K. Jiao, B. Zhou, P. Quan, J. Power Sources 154 (2006) 124–137.
[9] K. Jiao, B. Zhou, P. Quan, J. Power Sources 157 (2006) 226–243.
[10] H. Wu, P. Berg, X. Li, J. Power Sources 165 (2007) 232–243.
[11] X.G. Yang, F.Y. Zhang, A.L. Lubawy, C.-Y. Wang, Electrochem. Solid State Lett. 7 (2004) A408–A411.
[12] H. Masuda, K. Ito, T. Oshima, K. Sasaki, J. Power Sources 177 (2008) 303–313.
[13] I.S. Hussaini, C.-Y. Wang, J. Power Sources 187 (2009) 444–451.
[14] R. Satija, D.L. Jacobson, M. Arif, S.A. Werner, J. Power Sources 129 (2004) 238–245.
[15] D. Kramer, J. Zhang, R. Shimoi, E. Lehmann, A. Wokaun, K. Shinohara, G.G. Scherer, Electrochim. Acta 50 (2005) 2603–2614.
[16] A. Turhan, K. Heller, J.S. Brenizer, M.M. Mench, J. Power Sources 160 (2006) 1195–1203.
[17] S. Tsushima, K. Teranishi, S. Hirai, Electrochem, Solid State Lett. 7 (2004) A269–A272.
[18] K.R. Minard, V.V. Viswanathan, P.D. Majors, L.-Q. Wang, P.C. Rieke, J. Power Sources 161 (2006) 856–863.
[19] Z.W. Dunbar, R.I. Masel, J. Power Sources 182 (2008) 76–82.
[20] J. Wu, X.Z. Yuan, H. Wang, M. Blanco, J.J. Martin, J. Zhang, Int. J. Hydrogen Energy 33 (2008) 1747–1757.
[21] A.D. Bosco, M.H. Fronk, U.S. Patent 6,103,409 (2000).
[22] F. Barbir, H. Gorgun, X. Wang, J. Power Sources 141 (2005) 96–101.
[23] H.P. Ma, H.M. Zhang, J. Hu, Y.H. Cai, B.L. Yi, J. Power Sources 162 (2006) 469–473.
[24] K. Ito, K. Ashikaga, H. Masuda, T. Oshima, Y. Kakimoto, K. Sasaki, J. Power Sources 175 (2008) 732–738.
[25] J. Stumper, M. Löhr, S. Hamada, J. Power Sources 143 (2005) 150–157.
[26] S.G. Kandlikar, Z. Lu, T.Y. Lin, D. Cooke, M. Daino, J. Power Sources 194 (2009) 328–337.
[27] R.W. Hornbeck, Appl. Sci. Res. 13 (1964) 224–232.
[28] MATLAB Help archive.
[29] J. Chen, B. Zhou, J. Power Sources 177 (2008) 83–95.